The motion of a foam lamella traversing an idealised bi-conical pore with a rounded central region

Ferguson, D. J.; Cox, S. J.

Published in:
Colloids and Surfaces A: Physicochemical and Engineering Aspects

DOI:
10.1016/j.colsurfa.2013.02.015

Publication date:
2013

Citation for published version (APA):
Ferguson, D. J., & Cox, S. J. (2013). The motion of a foam lamella traversing an idealised bi-conical pore with a rounded central region. *Colloids and Surfaces A: Physicochemical and Engineering Aspects*, *438*, 56-62. https://doi.org/10.1016/j.colsurfa.2013.02.015

The motion of a foam lamella traversing an idealised bi-conical pore with a rounded central region

D.J. Ferguson, S.J. Cox

Institute of Mathematics and Physics, Aberystwyth University, Aberystwyth SY23 3BZ, UK

Abstract

The non-smooth motion of a single foam lamella traversing an idealised rock pore can lead to a significant pressure drop. We vary two parameters defining the shape of a biconical pore in two dimensions, and use Surface Evolver simulations and geometric arguments to demarcate the four different types of possible motion. We predict the transitions between different-shaped pores in which the lamella makes a symmetric or an asymmetric jump, an asymmetric crawl, or undergoes smooth motion. We give the time-averaged pressure drop as a function of pore shape.

1. Introduction

Foam is widely used in the oil industry for enhanced oil recovery (EOR) and as a proppant-carrying fluid for hydraulic fracturing. Pumping a gas into an oil reservoir to displace the oil into the production wellbore suffers from two significant problems: gravity override, in which the less dense gas simply rides over the oil in the reservoir, and channelling, where the gas simply chooses the easiest path and bypasses the oil trapped in less permeable regions. The use of a foam instead of a gas offers the possibility to control the mobility of the injected fluids, and thus to improve the efficiency of the sweep, as first noted over fifty years ago [1].

There have been several approaches to investigating the behaviour, and particularly the flow, of foams in porous media. One involves the controlled injection of gas and surfactant into sandstone cores, beadpacks and sandpacks, and measuring quantities such as the effluent bubble size, the pressure gradient, the fractional flows of gas and liquid, and the displacement of residual fluids; for example Bertin *et al.* [2] injected gas and surfactant into a heterogeneous porous medium consisting of a sandstone core surrounded by sand. The difference in permeability between the sand and the sandstone was 67 to 1, and the experiment was performed both with and without cross-flow between the two regions. With cross-flow, the foam flow rate was equalized in both regions, in spite of the differing permeabilities, so that an effective expulsive foam front moved through the entire block. Without cross-flow, it was observed that flow rates were higher in the low-permeability sandstone region. It is this behaviour which holds the key to a foam's usefulness as a drive fluid in EOR.

Measurements of effluent bubble sizes [3] have demonstrated that bubble size is about as large or larger than the pore bodies in the medium, and that even pre-generated foam had its texture altered by the porous medium. Hence the accepted view is that a foam flows through a porous medium as a train of bubbles, separated by foam lamellae which span the pores. The bubble trains take winding paths between regions of trapped gas and rock grains, as shown schematically in fig. 1(a).

This suggests a different approach, namely, to investigate events at the scale of the pores, and to determine the motion of individual bubbles or lamellae. A natural way to model a porous structure is as a bundle of narrow capillaries. An investigation of flow in uniform smooth capillaries [5] identified foam texture (i.e. bubble size and its distribution) as the most important factor in determining the effective foam viscosity, both for bulk and confined foams. Studying the flow of single lamellae in straight tubes allows an exploration of the effects of dissipation, particularly those due to the motion of Plateau borders in contact with the walls of the channels [6].

Rock pores are rarely straight, with uniform diameter, however. Rossen [7, 8, 9] considered flow through a more complicated pore shape, constructing a theory for the minimum pressure gradient required to maintain foam flow in

Email address: djf7@aber.ac.uk (D.J. Ferguson)

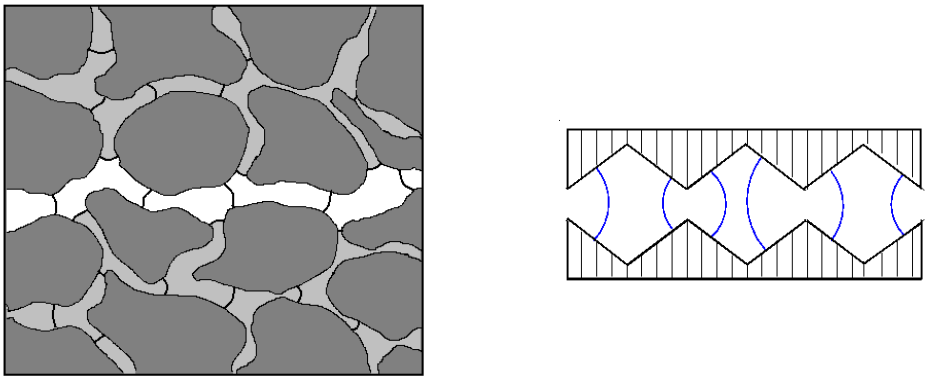

(a) (b)

Figure 1: (a) Bubbles flowing between trapped gas and rock grains in a porous medium. (b) A train of lamellae in an idealised porous medium.

a bi-conical pore. In his experiments, the lamella were found to jump across the centre of the pore, often forming strongly curved shapes straddling the middle of the pore, resulting in an additional contribution to the resistance over that expected for smooth lamella motion, and therefore a higher pressure drop for pores with a higher ratio of body-to-throat size. Rossen also evaluated the effects of compressibility (which increases the minimum pressure gradient) and interactions with stationary lamellae trapping gas in adjacent pores (which could reduce it to zero). He showed that even in two dimensions (2D) the qualitative features of the three-dimensional (3D) problem are retained.

Cox *et al.* [10] simulated the motion of a lamella through the same idealised bi-conical pore, both in 2D and 3D, using the Surface Evolver program. The results in 2D were in agreement with Rossen's earlier analysis, validating the simulations, and in 3D were used to show that when a lamella undergoes an asymmetric jump (as described in more detail below) the time-averaged pressure difference is again higher than expected for smooth lamella motion.

In this work we return to the 2D problem and explore the parameter space – the ratio of body-to-throat size and amount of trapped liquid in the pore – further in the Surface Evolver. We describe our assumptions and the geometry of the idealised pore in §2; in particular, the rounded region of the pore body differs slightly from previous work and we find that this influences the time-averaged pressured drop. The different lamella behaviour found in the simulations is given in §3, and in §4 we derive analytically the relationships between the parameters that demarcate the different behaviour.

2. Methods

2.1. The idealised problem

Rossen [7, 8, 9] assumed that the train of lamellae passed through a series of bi-conical sections, as illustrated in fig. 1(b). One section is illustrated in fig. 2 with a single lamella shown emerging from the throat.

In simulating the passage of the lamella through this bi-conical pore, the following assumptions are made:

(i) The flow is slow enough that a quasi-static model is appropriate, thus viscous drag of the lamella ends on the pore wall is negligible and the contact angle is constant at 90°;

(ii) The gas is incompressible, does not diffuse through the lamellae, and enters the pore at constant flow rate;

(iii) The surface tension of a lamella is constant, thus surface tension gradients are neglected.

We infer therefore that the lamellae obey Plateau's equilibrium laws [11], which are a consequence of the fact that a soap film tries to minimize its surface energy, equivalent here to its length. In our 2D case this means that the lamella

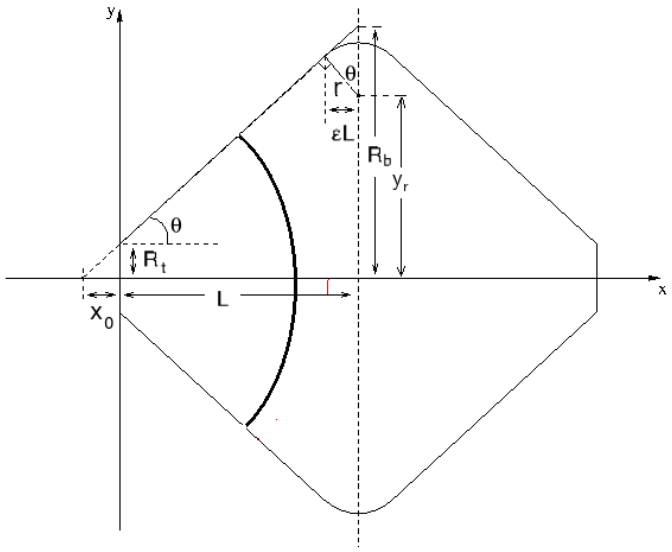

Figure 2: The geometry of the idealised bi-conical pore, with a single lamella shown as a thick line.

is an arc of a circle (which includes a straight line, corresponding to zero pressure difference) which meets the pore wall at $90°$. The assumption of constant flow rate allows us to view each increment in the volume of the "bubble" behind a lamella as a time step.

The shape of the pore is defined by its length L, the size of the pore throat R_t, and the angle at which the pore opens θ, shown in fig. 2. The sharp corners at the top and bottom of the pore body are rounded over a distance $2\epsilon L$ to represent the effects of pre-existing liquid in the pore, which would fill the smallest spaces and form a continuous wetting film coating the pore walls [3, 4]. We fix $L = 1$ and $R_t = 0.2$, set surface tension $\gamma = 1$ w.l.o.g., and consider the effect of varying θ and ϵ on the motion of a lamella and the time-averaged pressure drop.

The upper boundary of the pore is described piecewise:

$$y(x) = \begin{cases} x\tan\theta + R_t & \text{for } x \in [0, (1-\epsilon)L], \\ y_r + \sqrt{r^2 - (x-L)^2} & \text{for } x \in ((1-\epsilon)L, (1+\epsilon)L), \\ -x\tan\theta + 2R_b - R_t & \text{for } x \in [(1+\epsilon)L, 2L]. \end{cases} \tag{1}$$

The circular arc describing the central rounded part of the boundary has radius r and centre at (L, y_r), with

$$r = \frac{\epsilon L}{\sin\theta}, \tag{2}$$

$$y_r = R_t + L\tan\theta - \epsilon L\left(\tan\theta + \frac{1}{\tan\theta}\right). \tag{3}$$

The lower boundary is a reflection of the upper boundary in the horizontal x-axis.

2.2. Surface Evolver simulations

The Surface Evolver [12] is a program for modelling surfaces shaped by surface tension subject to volume and boundary constraints. Our constraints are the fixed walls of the pore, and the volume (area) enclosed behind (to the left of) the lamella.

We simulate gas entering the pore from the left and pushing the lamella to the right. The pressure difference across the lamella is given by the Young-Laplace equation [11]:

$$\Delta p = \frac{2\gamma}{r_l}, \tag{4}$$

where r_l is the radius of curvature of the lamella. The simulation starts with the lamella at the left side of the pore enclosing a bubble of volume $0.1V_{tot}$, where V_{tot} is the total volume of the pore. Each quasi-static iteration consists of increasing the bubble volume by a small amount $\frac{1}{200}V_{tot}$ and calculating the new lamella shape and position; we then record the volume of the bubble, expressed as a fraction of V_{tot}, the x coordinates of the ends of the lamella (the points at which the lamella meets the upper and lower walls), the length of the lamella, and the pressure difference across it.

Since we increase the volume behind the bubble by a fixed amount, each step represents a unit of time. The average pressure difference across a lamella during its motion through the pore therefore gives a time-averaged pressure drop Δp^{avg}. This can also be thought of as a population average for the pressure drop across a series of lamellae [7]. We take the average over the volume interval $[0.1V_{tot}, 0.9V_{tot}]$, noting that provided the lamella has returned to a symmetric arc far downstream, the contributions to the pressure drop at low and high bubble volumes cancel out, i.e.

$$\Delta p^{avg} = \frac{1}{V_{tot}} \int_0^{V_{tot}} p dV = \frac{1}{0.8V_{tot}} \int_{0.1V_{tot}}^{0.9V_{tot}} p dV. \tag{5}$$

To survey the parameter space, we increase θ from $\frac{\pi}{110}$ to $\frac{30\pi}{110}$ (measured in radians) in 30 steps, and ϵ from 0.02 to 0.98 in 49 steps, running a single simulation for each (θ, ϵ) pair.

3. Results

Varying the two parameters θ and ϵ produces four different types of behaviour:

Case (i) Smooth traverse

At large ϵ, for example, the pore is very rounded and the lamella travels smoothly across the pore, maintaining up-down symmetry throughout the motion. The average pressure difference across it is zero since the time it spends with a positive pressure difference, as it moves towards the body of the pore is balanced by the time spent with a negative pressure difference after it passes the pore body.

This is evident in the symmetrical pressure-time graph (fig. 3(d)), where it is also possible to see the point at which the lamella enters the rounded region of the pore from the change in slope.

Case (ii) Symmetric jump

For smaller ϵ, for example, the lamella jumps across the body of the pore when its ends reach the rounded region. It then assumes a symmetric shape again, but now curving backwards. We refer to this as a symmetric jump. Fig. 4 shows the lamella positions, and the pressure-volume graph is shown in fig. 3(a). Since the jump occurs after the bubble volume is half the pore volume, this jump leads to a non-zero time-averaged pressure drop.

Case (iii) Asymmetric jump

In certain cases, when the ends of the lamella reach the rounded part of the pore it jumps not in a symmetric way but in an asymmetric way, leading to a lamella that straddles the body of the pore. This usually occurs for ϵ slightly larger than for the symmetric jump (although it can also be triggered by the introduction of a little asymmetry in the shape of the pore of lamella). When the trailing end of the lamella reaches the rounded part, the lamella jumps back to a symmetric position as in the cases above. Fig. 5 illustrates the lamella positions before and after each jump, and the associated pressure-volume graph is shown in fig. 3(b). Note how the pressure drop is zero while the lamella is straight. An asymmetric jump also leads to a non-zero time-averaged pressure drop.

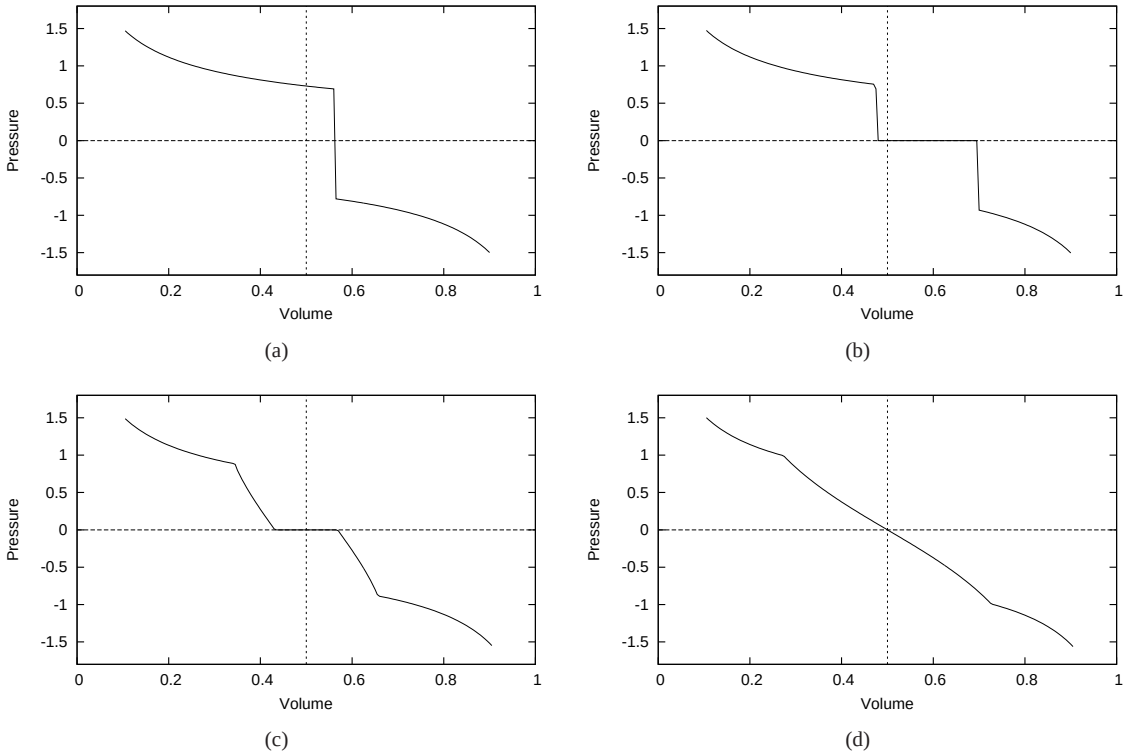

Figure 3: Pressure *vs.* volume graphs for the motion of the lamella through the pore, with $\theta = \frac{\pi}{5}$. (a) Symmetric jump, with $\epsilon = 0.10$. (b) Asymmetric jump, with $\epsilon = 0.20$. (c) Asymmetric crawl, with $\epsilon = 0.36$. (d) Smooth traverse, with $\epsilon = 0.46$.

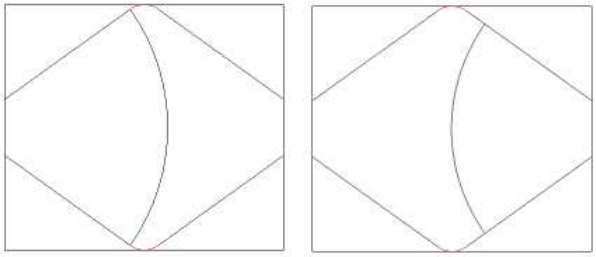

Figure 4: Lamella positions before and after the *symmetric* jump with $\theta = \frac{\pi}{5}$ and $\epsilon = 0.1$.

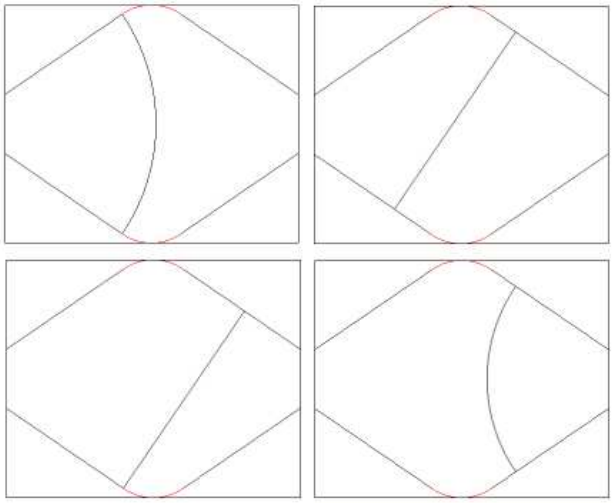

Figure 5: Lamella positions before and after an *asymmetric* jump with $\theta = \frac{\pi}{5}$ and $\epsilon = 0.2$.

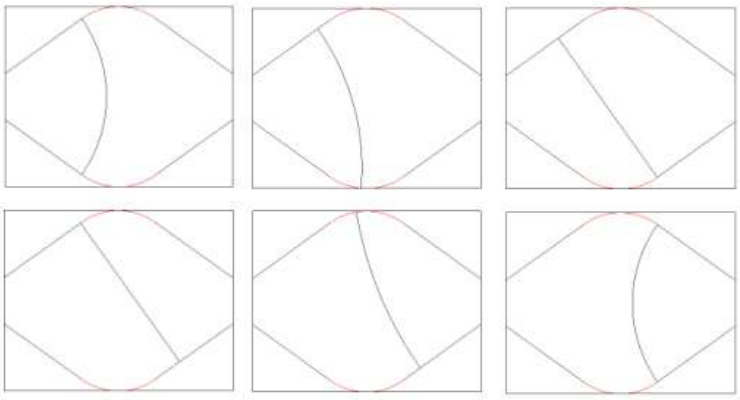

Figure 6: Lamella positions during an asymmetric crawl with $\theta = \frac{\pi}{5}$ and $\epsilon = 0.36$.

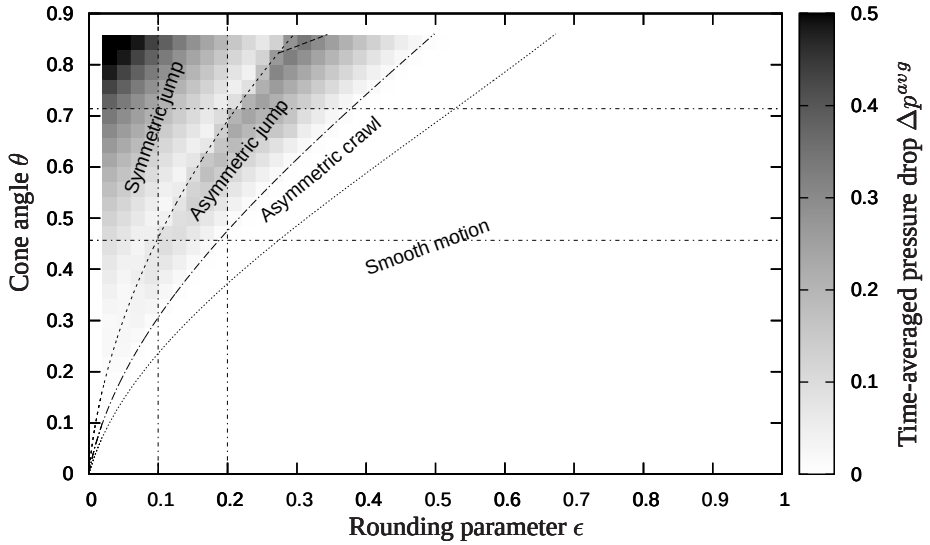

Figure 7: The time-averaged pressure drop for all values of θ and ϵ considered here, with the three demarcation curves, eqs. (8), (13) and (15) shown emanating from the origin. The vertical and horizontal lines are the lines along which the data is plotted in fig. 8

Case (iv) Asymmetric crawl

A case that we believe we have identified for the first time is intermediate between cases (i) and (iii): when the lamella reaches the rounded part of the pore, one end crawls across the rounded region first, with the other moving backwards a little distance. The lamella then continues to move asymmetrically until the trailing end reaches the rounded part. The trailing end then crawls across the middle, until symmetry is restored. The time-averaged pressure drop is zero in this case.

The sequence of lamella shapes is shown in fig. 6, and the associated pressure-volume graph is shown in fig. 3(c). We emphasise that each lamella shape is an equilibrium film shape, and that this behaviour is *not* due to poor convergence. (In technical terms, we assessed this from the eigenvalues of the Hessian of energy [9, 13].)

4. Demarcating the different types of behaviour

The results of 1470 simulations varying θ and ϵ are summarised in fig. 7, in terms of the time-averaged pressure drop Δp^{avg}.

For large ϵ the lamella always moves smoothly through the pore. As ϵ decreases, the asymmetric crawl appears, first at high θ (narrow, tall, pores), occupying a rather narrow band. There is another narrow band in which the asymmetric jump is observed, and then at small ϵ we find the symmetric jump. In the two regions where the jumps occur, there are distinct bands of high Δp^{avg}.

We now give analytic expressions for the three curves which demarcate the different behaviours shown on fig. 7.

4.1. Pore volume

Recall that at any instant in time, that is for any given bubble volume, the lamella minimizes its length and meeting the pore wall at 90°.

The total volume of the bi-conical pore is

$$V_{tot} = 4R_t L + 2L^2 \tan\theta + \frac{2\theta\epsilon^2 L^2}{\sin^2\theta} - \frac{4\epsilon^2 L^2}{\sin 2\theta}. \tag{6}$$

4.2. Constraints

Not all values of θ and ϵ give rise to physically-realistic motion because it is possible that the lamella does not remain confined within the pore in the way that we describe. For example, it is possible that when the lamella is in the asymmetric configuration, one of its ends may emerge from the downstream end of the pore, before the lamella jumps back to the symmetric configuration. This occurs when

$$\epsilon < R_t \sin 2\theta - \cos 2\theta. \tag{7}$$

This is visible as a short dashed line at the top of the asymmetric jump region on fig. 7, and clearly has little influence on our results.

It is also possible that as the forward-bulging lamella reaches the rounded region of the pore body, it may intersect the downstream part of the pore boundary part-way along its length. However, this does not happen for the values of θ and ϵ considered here.

4.3. Symmetric to asymmetric jump

The symmetric jump occurs for small values of ϵ. If the bubble volume $V_b(x)$ when the ends of the lamella reach the rounded part of the pore (i.e. when $x = (1-\epsilon)L$) is less than half the total pore volume, then the lamella is unable to make a symmetric jump because its area would then have to be greater than half the pore volume. The symmetric jump therefore can only occur up to the point at which

$$V_b((1-\epsilon)L) = \frac{V_{tot}}{2}. \tag{8}$$

This statement is equivalent to Rossen's criteria [9], that there is a turning point in the graph of x *versus* V_b. If the value of V_b is lower, then an asymmetric jump occurs.

While $x \leq (1-\epsilon)L$ the radius of curvature of the lamella (cf. fig. 2) is

$$r_l(x) = \sqrt{\left(x + \frac{R_t}{\tan\theta}\right)^2 + \left(x\tan\theta + R_t\right)^2} = \frac{x}{\cos\theta} + \frac{R_t}{\sin\theta}, \tag{9}$$

and the bubble volume is

$$V_b(x) = \theta r_l(x)^2 - \frac{R_t^2}{\tan\theta}. \tag{10}$$

At $x = (1-\epsilon)L$ we therefore have

$$V_b((1-\epsilon)L) = \theta\left(\frac{(1-\epsilon)L}{\cos\theta} + \frac{R_t}{\sin\theta}\right)^2 - \frac{R_t^2}{\tan\theta}. \tag{11}$$

Eqs. (6) and (11) together mean that eq. (8) is an implicit expression for ϵ and θ, and is the leftmost of the three curves plotted on fig. 7; it correctly separates the regions in which the two jumps are found to occur in the simulations.

4.4. Asymmetric jump to crawl

The asymmetric jump only occurs if $V_b((1-\epsilon)L) < \frac{1}{2}V_{tot}$ and if the arc length of the lamella, at the point where its ends meet the beginning of the rounded region of the pore wall ($x = (1-\epsilon)L$), is greater than the lamella's (straight line) length in the asymmetric configuration.

The straight line length is given by $2L\sin\theta + 2R_t\cos\theta$, independent of ϵ, while the length of the arc is $2\theta r_l((1-\epsilon)L)$, with r_l given by eq. (9). Thus the critical parameters are implicitly determined by the inequality

$$2\theta\left(\frac{(1-\epsilon)L}{\cos\theta} + \frac{R_t}{\sin\theta}\right) \geq 2L\sin\theta + 2R_t\cos\theta. \tag{12}$$

This can be rearranged to give an expression for the critical value of ϵ, in terms of θ, at which the behaviour changes from the asymmetric jump to the asymmetric crawl:

$$\epsilon = 1 + \frac{R_t}{L\tan\theta} - \frac{\sin 2\theta}{2\theta} - \frac{R_t\cos^2\theta}{L\theta}. \tag{13}$$

This is the middle of the three curves plotted on fig. 7, in agreement with the simulation results.

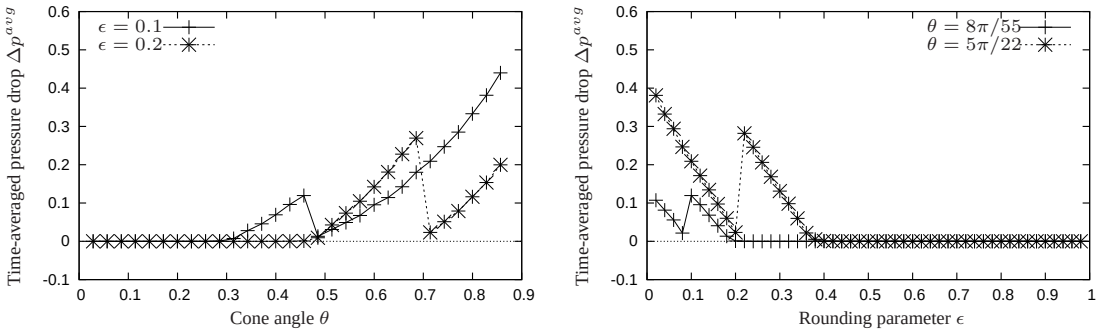

Figure 8: Variation in the time-averaged pressure drop for fixed (a) ϵ or (b) θ.

4.5. Asymmetric crawl to smooth motion

The straight-line lamella configuration is not attainable when the radius of curvature of the rounded part of the pore wall is greater than the height of the pore (i.e. when the centre of the arc lies below the x-axis). Thus the asymmetric crawl is replaced by smooth motion of the lamella when

$$r = y(L), \tag{14}$$

where r and $y(x)$ are as given in eqs. (1) and (3). Rearranging gives

$$\theta = \tan^{-1}\left(\frac{R_t - \sqrt{R_t^2 - 4\epsilon(\epsilon-1)}}{2(\epsilon-1)}\right). \tag{15}$$

This is the right hand curve plotted in fig. 7, and agrees with the results of the simulation in demarcating the asymmetrical crawl from the smooth motion of the lamella.

5. Discussion

We have shown how the different behaviours vary with the pore angle θ and the rounding parameter ϵ and offered explanations for why these changes occur. Our main result is fig. 7, showing that the time-averaged pressure drop is only non-zero if the lamella jumps, and that in these cases the pressure drop broadly increases as θ increases and ϵ decreases, that is for pores that are from from being straight and contain little residual fluid. Fig. 8 shows how the average pressure drop varies with θ for fixed ϵ and *vice versa* (along the horizontal and vertical lines marked on fig. 7). Note how the time-averaged pressure drop falls almost to zero around the transition from a symmetric to an asymmetric jump, but that the largest pressure drops are caused by the symmetric jump.

Rossen [7, 8, 9] studied a pore in which the rounded region was defined by a sinusoidal function, rather than a circular arc (eq. 1). This changes the slope of the pore wall in the rounded region, and thus the lamella shape for given volume. To make comparison with that work, we show in fig. 9 our results for this geometry, which should be compared with fig. 8. Changing the geometry to be sinusoidal has a significant quantitative effect on the parameter values for which the jumps occur and hence on the time-averaged pressure drop. In particular, symmetric jumps now only occur for very small ϵ, while asymmetric jumps occur for a larger range of ϵ. Thus, in the sinusoidal case, it is the asymmetric jump that leads to the greatest pressure drops, and they are greater in magnitude than in the circular arc case.

Beyond the quasi-static limit of slow lamella motion, friction at the ends of a lamella, where it meets the pore wall, will become important [14]. It may even be sufficient to suppress the jumps entirely, in which case viscous forces will be the only contribution to the time-averaged pressure drop. Then it will be the length of the pore walls that determine this quantity, not its shape.

Nguyen *et al.* [15] performed a similar set of experiments to Rossen using a model glass pore; they made direct measurements of the pressure at either end, and compared these to the predictions of a model which incorporates

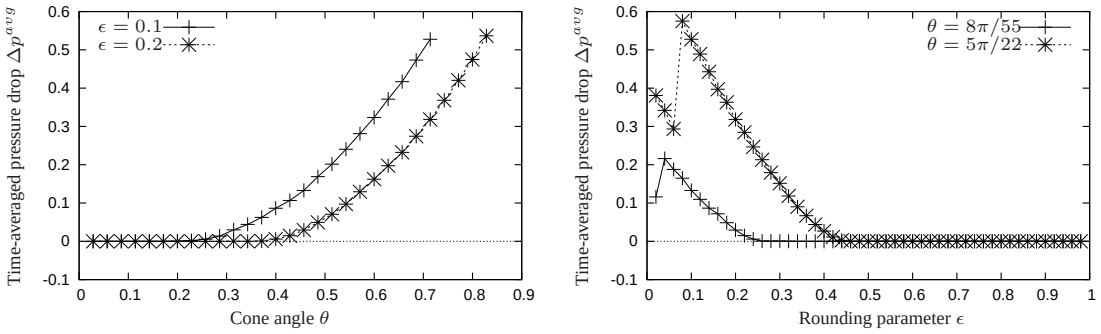

Figure 9: Variation in the time-averaged pressure drop for a pore with a sinusoidally curved body. Two different values of (a) ϵ (cf. fig. 8(a)), where here the data covers only the asymmetric jump, and (b) θ (cf. fig. 8(b)).

dynamic effects such as viscous drag and surface tension gradients due to the stretching and contracting of the lamella. Their results suggest that the quasi-static model significantly underestimates the pressure difference, especially in the diverging section of the pore.

A model that accounts for the redistribution of surfactant, such as the one developed by Kraynik and Hansen [16], and therefore the variation in surface tension, is required. Such variations in surface tension will affect the instantaneous pressure difference across the film (eq. (4)), and therefore the time-averaged pressure drop, introducing further asymmetry into the pressure time graph, in addition to possible jumps.

Incorporating these dynamic effects into a Surface Evolver simulation requires an understanding of how the foam structure is distorted from the equilibrium conditions given by Plateau's rules. A 2D viscous froth model for dry bulk foam is described in [17], which allows the lamellae to be distorted from a circular arc by a viscous drag force. The distortions due to drag have also been investigated experimentally [20] for single lamellae in straight tubes of varying cross-section.

Other effects which need to be examined are diffusion (which has recently been investigated in [18]) and the interactions with stationary lamellae [19], as well as moving lamellae which merge during the motion through the pore, observed experimentally in [15].

Acknowledgements

We thank Ken Brakke for guidance on Surface Evolver. This research is funded by the FP7 Marie Curie IAPP Project PIAP-GA-2009-251475-HYDROFRAC.

References

[1] A. Fried, Foam-drive process for increasing the recovery of oil, Tech. rep., U.S. Bureau of Mines (1967).

[2] H.J. Bertin, O.G. Apaydin, L. Castanier, A. Kovscek, Foam flow in heterogeneous porous media: Effect of crossflow, SPE **4** (1999) 75–82.

[3] A. Kovscek, C.J.Radke, Fundamentals of foam transport in porous media, Tech. rep., University of California, Berkeley (1993).

[4] W.R. Rossen, Theories of Foam Mobilization Pressure Gradient, SPE 17358 (1988)

[5] G. Hirasaki, J. Lawson, Mechanisms of foam flow in porous media: Apparent viscosity in smooth capillaries, SPE **25** (1985) 176–190.

[6] I. Cantat, N. Kern, R. Delannay, Dissipation in Foam Flowing Through Narrow Channels, EPL **65** (2004) 726–732

[7] W.R. Rossen, Theory of Mobilization Pressure Gradient of Flowing Foams in Porous Media I: Incompressible Foam, J. Coll. Interf. Sci. **136** (1990) 1–16.

[8] W.R. Rossen, Theory of Mobilization Pressure Gradient of Flowing Foams in Porous Media II: Effects of Compressibility, J. Coll. Interf. Sci. **136** (1990) 17–37.

[9] W.R. Rossen, Theory of Mobilization Pressure Gradient of Flowing Foams in Porous Media III: Asymmetric Lamella Shapes, J. Coll. Interf. Sci. **136** (1990) 38–53.

[10] S.J. Cox, S. Neethling, W. Rossen, W. Schleifenbaum, P. Schmidt-Wellenburg, J. Cilliers, A theory of the effective yield stress of foam in porous media: the motion of a soap film traversing a three-dimensional pore, Colloids and Surfaces A: Physicochem. Eng. Aspects **245** (2004) 143–151.

[11] D. Weaire, S. Hutzler, The Physics of Foams, Oxford University Press, 1999.

[12] K. Brakke, The Surface Evolver, Exp. Math. **1** (1992) 141–165.

[13] K. Brakke, The Surface Evolver and the stability of liquid surfaces, Phil. Trans. R. Soc. A **354** (1996) 2143–2157.

[14] Q. Xu, W.R. Rossen, Effective Viscosity of Foams in Periodically Constricted Tubes, Colloids and Surfaces A: Physicochem. Eng. Aspects **216** (2003) 175–194.

[15] Q. Nguyen, P. Currie, P. Zitha, Motion of foam films in diverging-converging channels, Colloid and Interface Science **271** (2004) 473–484.

[16] A.M. Kraynik, M.G. Hansen, Foam rheology: A model of viscous phenomena, J. Rheol. **31** (1987) 175–205.

[17] N. Kern, D. Weaire, A. Martin, S. Hutzler, S.J. Cox, Two-dimensional viscous froth model for foam dynamics, Phys. Rev. E **70** (2004) 041411.

[18] L.E. Nonnekes, S.J. Cox, W.R. Rossen, A 2D Model for the Effect of Gas Diffusion on Mobility of Foam for EOR, Proc. 13th European Conference on the Mathematics of Oil Recovery, Biarritz, France, 2012.

[19] W.R. Rossen, Minimum Pressure Gradient for Foam Flow in Porous Media: Effect of Interactions with Stationary Lamellae, J. Coll. Interf. Sci. **139** (1990) 457–467.

[20] B. Dollet, I. Cantat, Deformation of soap films pushed through tubes at high velocity, J. Fluid Mech. **652** (2010) 529–539.